

MEASUREMENT OF THE THERMAL CONDUCTIVITY OF CRYSTALLINE He⁴

L. P. MEZHOV-DEGLIN

Institute for Physics Problems and Institute of Solid State Physics, Academy of Sciences, U.S.S.R.

Submitted to JETP editor January 29, 1965

J. Exptl. Theoret. Phys. (U.S.S.R.) 49, 66-79 (July, 1965)

The thermal conductivity of crystalline He⁴ is measured in the range 0.5°–2.5° K at pressures up to 185 atm. The samples were grown in a glass vial at constant pressure with continuous visual and temperature control. Single crystals having a low concentration of lattice defects were obtained. The temperature dependence and maximum thermal conductivity of these single crystals differ greatly from the ordinarily observed properties, and agree closely with the results obtained in Gurzhi's theoretical study of transfer processes in ideal crystals.^[15]

1. INTRODUCTION

SOLID He³ and He⁴ are ideal objects for the study of heat transfer processes in dielectric crystals. Chemical impurities are entirely absent from helium, which can be prepared in the form of very pure isotopes, and the elastic properties of helium crystals can be modified greatly by applying relatively low pressures. With a pressure increase from 25 to 250 atm the density of He⁴ crystals increases 25% while the lattice symmetry remains unchanged, and the Debye temperature is doubled.

The thermal conductivity of solid He⁴ was first measured by Webb et al.^[1] However, the method of capillary blocking used by these investigators did not permit control of the crystal growth process. In addition, as the helium solidified the pressure in the working vial changed considerably; this must have essentially changed the quality of the samples. The presence of defects in such samples was later confirmed by the 12-fold increase of their thermal conductivity after annealing, as observed in^[2].

Shal'nikov^[3,4] has developed a technique that permits direct observation of helium solidification in a glass piezometer. The possibility of growing crystals under constant pressure with continuous control has made this method most suitable for achieving our goal of preparing and investigating the most perfect He⁴ crystals that can be produced.^[5]

2. APPARATUS

The apparatus used for our measurements is

represented in Fig. 1. A helium Dewar contained a vacuum chamber A within which we placed a glass vial for growing solid helium crystals. A German silver capillary shielded by a Dewar jacket connected the vial to the filling system, which included a helium gasifier^[6] with a working volume of 9 cm³ that could raise the pressure in the vial to 200 atm, a standard manometer M₁

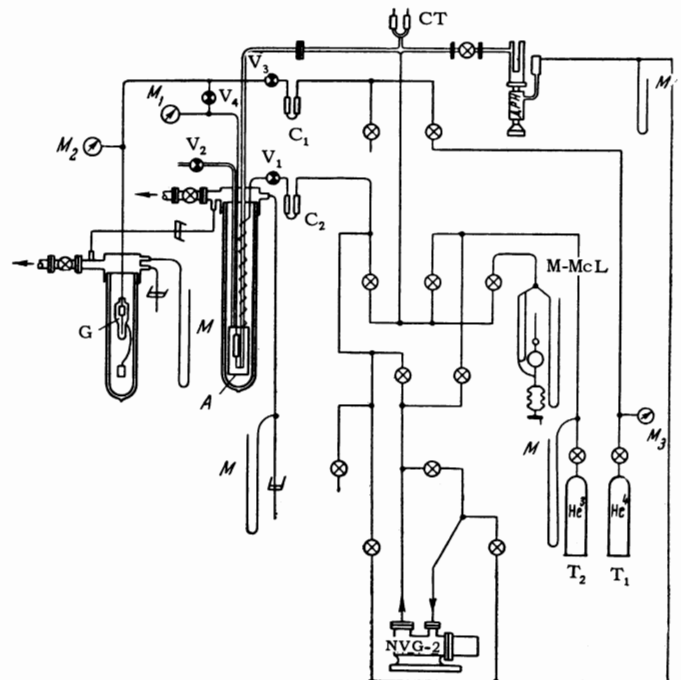


FIG. 1. Diagram of apparatus. A – glass vacuum chamber containing vial for growing He⁴ crystals; T_{1,2} – metal tanks for storing pure gas; V_{1,2,3,4} – metal sylphon valves; G – helium gasifier; D – mercury diffusion pump; C_{1,2} – charcoal traps; M – mercury manometers; M_{1,2,3} – metal manometers; M-McL – McLeod gauge; NVG-2 – forepump.

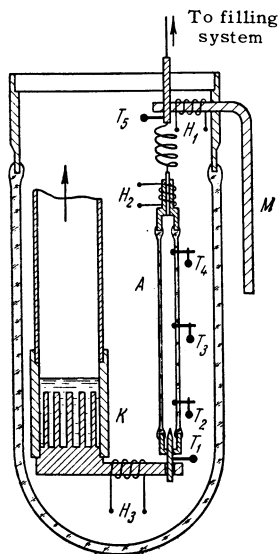


FIG. 2. Arrangement of parts inside the vacuum chamber. A – glass vial; K – cryostat; M – thermal bridge; $H_{1,2,3}$ – constantan heaters; $T_{1,2,3,4,5}$ – carbon resistance thermometers.

that monitored the pressure in the system, and the manometer M_2 of the gasifier. The metal siphon valves $V_{1,2,3,4}$ ^[7] in the filling system reliably controlled the flow at all working pressures. A 15-liter metal tank T_1 was used to store pure helium gas, which was fed during the experiments to the filling system through a highly purified charcoal trap C_1 cooled by liquid nitrogen.

Figure 2 is a diagram of the vacuum chamber containing the vial for growing solid He crystals. This vial was a test tube made of No. 29 chemical glass (2.45 ± 0.03)/4.5 mm in diameter and about 52 mm long. The end-sealing material was No. 47KhB iron-chromium alloy. A copper conductor of cold 2 mm in diameter was soldered into the bottom of the vial; its sharp upper end extended about 2 mm above the metal-glass seal. The cold conductor connected the vial to a copper cryostat^[8] of ~ 4 cm³ volume filled with liquid He³ or He⁴. By pumping out the liquid He³ vapor the temperature of the cryostat and of the crystal grown in the vial was lowered to 0.4°K. The constantan heater H_2 ($\sim 90 \Omega$) was wound around a copper cap that was soldered to the upper iron-chrome seal. A coiled German silver capillary 180 mm long and 0.15/0.40 mm in diameter connected the vial to the capillary of the filling system. Along a section located inside the vacuum chamber the filling system capillary communicated with an external helium bath through a massive copper cold conductor M soldered into and passing through the upper part of the vacuum

jacket. This thermal bridge served to carry off heat flowing upward along the filling capillary. The heater H_1 was used to warm the bridge in order to avoid blocking of the capillary during the growth of a crystal.

Three platinum wires 0.4 mm in diameters were sealed in the glass wall of the vial; the fused inside ends of these wires were in direct contact with the grown solid helium sample. The separations of the wires were ~ 21 mm; the lowest wire was located 6 mm from the metal-glass seal, and the uppermost wire was located 4 mm from the top seal. The carbon resistance thermometers $T_{2,3,4}$ that were soldered to the wires monitored the temperature distribution along the sample.

3. THERMOMETERS

The thermometers were flat disks ~ 0.5 mm thick cut from an Allen-Bradley carbon radio resistor (10Ω , 1 W). The surfaces of the disks were polished and then coated electrolytically with copper. Tin-plated constantan wires 0.07 mm in diameter were used as current and potential leads.

Figure 3 shows the calibration of one thermometer. The working current of the thermometers was $10 \mu\text{A}$ during measurements down to 1°K, and $1 \mu\text{A}$ at lower temperatures; therefore less than 10^{-7} W was developed in the thermometers. The dashed curve in Fig. 3 represents the thermometer calibration at low temperatures with a $10 \mu\text{A}$ current. Resistance was measured with a PMS-48 potentiometer; a F116/1 microvolt-microammeter was used as a null galvanometer. The relative accuracy of the measurements in

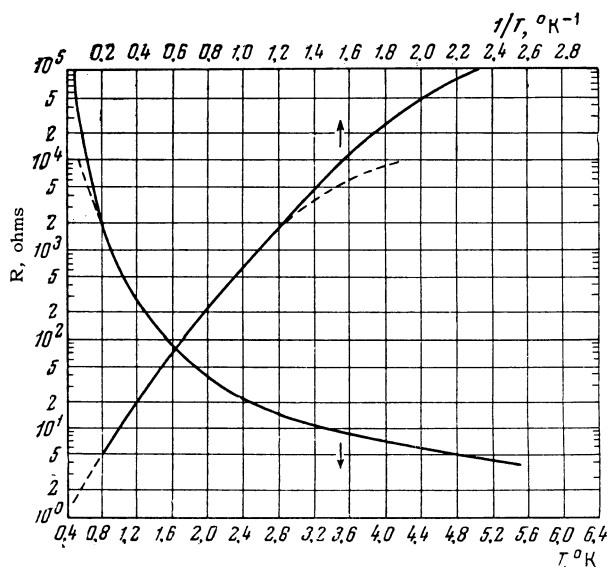


FIG. 3. Calibration of one thermometer.

the working range was $\Delta R/R \sim 10^{-4}$; at the lowest temperatures the relative accuracy was 10^{-3} .

The sensitivity of the thermometers can be represented by

$$\Delta R/R \approx (5/T)(\Delta T/T).$$

The measured temperature difference comprised only hundredths of a degree; in our calculations we therefore used more complicated interpolation formulas.^[9] In the 2.5°–0.8°K region the thermometer temperature was defined by

$$\log R + k/\log R = a + b/T,$$

while below 0.8°K a more suitable formula was

$$k'/\log R - \log R = b'T - a'.$$

The constants for one of the thermometers were

<i>a</i>	<i>b</i>	<i>k</i>	<i>a'</i>	<i>b'</i>	<i>k'</i>
0.95890	2.09706	0.67477	2.3570	19.600	56.180

When the thermometers inside the vacuum chamber had been subjected to several cycles of heating to room temperature and subsequent cooling practically no change of their properties was observed. Using the interpolation formulas, we calculated the difference between the temperature readings of two thermometers with at least $\pm 0.5 \times 10^{-3}$ °K accuracy in the 2.5°–0.7°K region. When the temperature dropped to 0.4°K the accuracy of the difference measurements became $\pm 1 \times 10^{-3}$ °K.

4. EXPERIMENT

A. Crystal growing. At the start of the experiment He⁴ gas from an outside tank was condensed in the working volume of the gasifier and inside the working bulb; the temperature within these parts was reduced to 1.3°K by pumping liquid helium vapor from the outer Dewars. When the bulb and gasifier were filled with the liquid the outside tank was closed off from the filling system. Pressure was generated in the system by heating the working volume of the gasifier; the rate of pressure increase did not exceed an average of 3 atm/min. To obviate blocking of the capillary connecting the vial to the filling system, the bridge temperature was maintained at a few tenths of a degree above the melting point at a given pressure. The temperature of the cryostat and of the lower part of the bulb was also gradually elevated with increasing pressure and was above the melting point. When a specified pressure had been reached the filling line of the vial was closed off from the gasifier; the vial then was connected only to the standard manometer (*M*₁ in

Fig. 1), which was filled with gas at the same pressure. Since the vial volume was much smaller than that of the Bourdon tube of the manometer, the relative pressure change in the vial-manometer system upon solidification of the liquid in the vial was less than 2%, so that crystallization occurred at a practically constant pressure.

Crystal growth was monitored in two ways, visually and by recording the temperature distribution along the vial. Using a binocular microscope ($\times 8$, with a depth of focus of about a millimeter) positioned outside and opposite the vial, we were thus able to observe how a layer of solid helium appeared on the surface of the copper needle inside the vial, duplicating the contour of the cold conductor at first. As the crystal grew its boundary was gradually smoothed out, so that about halfway between the cold conductor and the lower thermometer *T*₂ the phase interface became horizontal. The rate of crystal growth was regulated by varying the rate of cryostat cooling; under our conditions the optimal growth rate was 0.5–1 mm/min.

The purity of the initial gas was an important factor. In the first experimental run we used He⁴ collected from a Dewar containing boiling liquid helium at atmospheric pressure; we afterwards tested high-purity helium from the Ukhtinsk gas field. The best results were obtained in the third run, where superfluid He⁴ flowed through a tube filled with crocus before entering a metal tank *T*₁ at 2 atm. Crystals grown from helium purified in this manner exhibited high thermal conductivity on the average; the reproducibility of results was also improved.

As shown in^[3], with a slow rise of pressure in liquid He II in the region where the γ phase exists it is usually difficult to avoid the precipitation of "snow;" the snow increases in abundance with increasing impurity of the initial helium. The growth of a transparent γ crystal could only be observed with the creation of a considerable temperature gradient along the vial and a slow rise of pressure (less than 0.2 atm/min). However, the γ crystals could not be measured quantitatively because the crystals were grown in such a long vial that the temperature gradient exceeded the region in which this phase existed. With a pressure rise at constant temperature the γ crystal broke into pieces and melted, but another, more stable, α crystal grew rapidly underneath. When the temperature was lowered at constant pressure, then underneath, in the solid helium around the cold conductor, a boundary appeared which moved upward rapidly and overtook the in-

interface between the γ phase and the liquid. The upper part of the crystal then became clouded, cracks appeared, and the crystal broke into pieces and melted. A temperature analysis of transformations occurring in the lower part of the vial would require the positioning of several thermometers because of the low thermal conductivity of the three-phase system.

B. Measurements. The thermal conductivity of grown samples was measured statically. A constant downward heat flow along the vial resulted from heat generation in the constantan heater H_2 located near the upper part of the vial. Since the thermal resistance of the capillary leading to the thermal bridge exceeded the resistance of the vial by almost three orders of magnitude, practically all the heat generated in the heater was carried off through the solid helium filling the vial. The temperature distribution along the sample was measured with the thermometers $T_{2,3,4}$, while the temperature of the copper cold conductor was measured by the thermometer T_1 . The thermal conductivity of the portion of the sample located between the thermometers T_i and T_j was determined from the formula

$$K_{ij} = \dot{Q} / \Delta T_{ij}, \quad \Delta T_{ij} = T_i - T_j, \quad (1)$$

where \dot{Q} is the power developed in the heater. This power was determined from the thermal conductivity in a given range of temperatures and pressures, and was chosen to produce a temperature gradient of at least a few hundredths of a degree along the vial. In the region of maximum thermal conductivity and of the lowest temperatures the power development depended mainly on the cooling performance. In the second case the main obstacle to an increase of power was the temperature jump at the copper-solid helium interface, which exceeded the temperature difference along the vial by more than an order of magnitude.

For measurements above 1.2°K the vial and cryostat were cooled by pumping liquid He^4 vapor from an external bath; lower temperatures were produced by pumping He^3 from the cryostat. The temperature of the external bath was maintained constant to within better than 10^{-4} °K by means of a special temperature stabilizer.^[10] The temperature of the cryostat containing He^3 was stabilized by regulating the pumping rate with a valve at the entrance of the diffusion pump (Fig. 1).

For thermal conductivity measurements at about 0.45°K in a crystal grown at 60 atm and having the highest thermal conductivity in this region the accuracy of the measurements was

$\pm 20\%$ and was correspondingly increased for crystals having lower thermal conductivity. The average accuracy of K_{42} near its maximum was not worse than $\pm 10\%$.

5. EXPERIMENTAL RESULTS

Our first thermal conductivity measurements were performed on crystals grown in a vial 6 mm in diameter. The values obtained at relatively high temperatures (about 2°K) were close to the values obtained in^[1] for samples of corresponding densities; however, at lower temperatures we observed an extremely more rapid growth of thermal conductivity. The crystals were too wide for sufficient accuracy; therefore all subsequent thermal conductivity measurements were performed on samples grown in a vial of 2.5-mm diameter. The thermometer separations were $l_{43} = l_{32} = l_{42}/2 = 21$ mm, and the outer thermometers were located at distances equal to at least two diameters from the end of the crystal. The principal measurements were performed on crystals grown at 60, 85,¹⁾ 153, and 185 atm.

Figures 4 and 5 show the thermal conductivity measured in crystals grown at 85 and 185 atm. For convenience, the results are arbitrarily divided into three groups (I, II, and III) according to the slope of the high-temperature branch of the thermal conductivity curve and its behavior with decreasing temperature near the thermal conductivity maximum. Figure 4a shows the mean thermal conductivity K_{42} along the crystal that is typical for each of the three groups. For comparison, the dashed lines indicate the results obtained in^[2] for crystals having the same density before and after annealing. At 85 atm 12 crystals were investigated, of which four can be assigned to group I, five to group II, and three to group III. Figure 4,b–d shows separately the temperature dependence of thermal conductivity in the upper (K_{43} , dashed curve) and lower (K_{32}) parts of the crystal for the same samples as in Fig. 5a. Figure 4e shows, for comparison, the curves of the best crystal in group I.

Figure 5a shows the measurements obtained at 185 atm. The eight investigated crystals were assigned as follows: three to group I, two to group II, and three to group III. Figure 5b shows the thermal conductivity behavior for one crystal

¹⁾We originally grew crystals at 82 atm. The pressure was later raised to 85 atm for convenience in making comparison with results given by other authors. The accompanying change of crystal properties was insignificant.

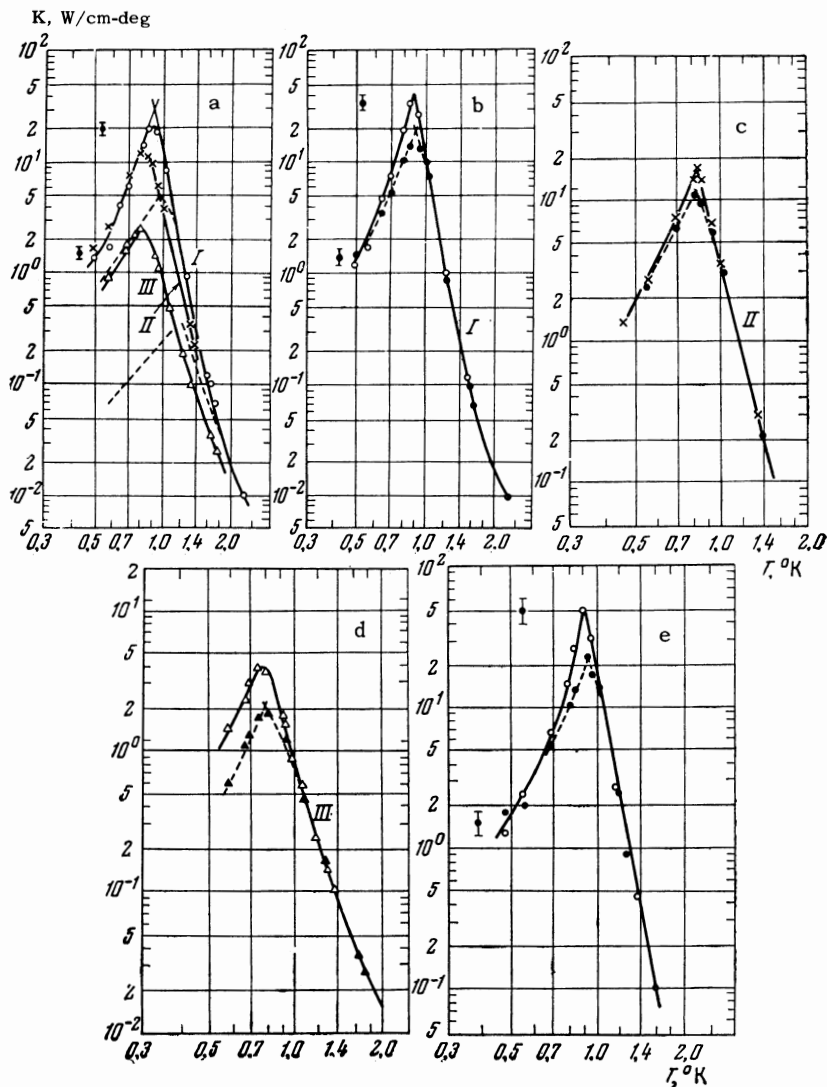


FIG. 4. Thermal conductivities of samples grown at 85 atm. a – general summary of results; the dashed curves represent the measurements in [2] for samples having the same density before and after (upper curve) annealing. b, c, d, – thermal conductivity of the upper (dashed curve) and lower parts of the same crystals. e – curve for the best sample in group I.

of group III.

In the graph representing the temperature dependence of the thermal conductivity for each of the crystals we can clearly distinguish both a high-temperature branch to the right of the maximum, where the thermal conductivity increases exponentially with decreasing temperature, and a low-temperature branch to the left of the maximum, where the thermal conductivity decreases as the temperature is lowered. In most cases the high-temperature branches of K_{43} and K_{32} for the upper and lower parts of a crystal diverge only near the maximum (Fig. 4, b–e); the maximum thermal conductivity K_{32}^{\max} in the lower part of the crystal is about twice the magnitude of K_{43}^{\max} . The corresponding curves show that the temperature region where the exponential rise is replaced by a weaker power law becomes broader as the maximum thermal conductivity is reduced.

Figure 5b shows an interesting case where the thermal conductivity differs in the upper and

lower parts of a crystal throughout the entire temperature range. The difference between the behaviors of K_{32} and K_{43} can evidently be accounted for by an increased concentration of

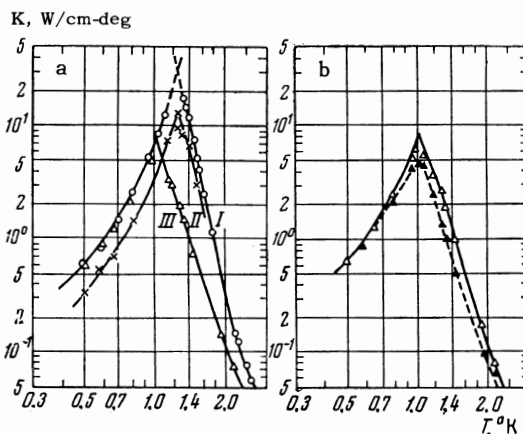


FIG. 5. Thermal conductivities of samples grown at 185 atm. a – general summary of results. b – thermal conductivity of the upper (dashed curve) and lower parts of one crystal in group III.

macroscopic defects accompanying the growth of the sample, such as occurs in zone purification. The way in which changes of lattice quality affect the thermal conductivity of a sample can be observed during the time of the measurements. Two or three cycles of measurements, in good mutual agreement, were usually obtained for a single crystal, on both sides of the maximum. In some instances of rapid crystal heating (faster than 0.1 deg/min) a reduced thermal conductivity near the maximum was observed during the subsequent cooling process. The transition from the high-temperature to the low-temperature branch became smoother, and the position of the maximum was shifted towards lower temperatures, while the position of the low-temperature branch remained unchanged. Rapid heating of a sample between cycles (faster than 0.5 deg/min) reduced its thermal conductivity over the entire temperature range; this result appears to be associated with macroscopic defects in the crystal.

Figure 6 shows the measurements of the average thermal conductivity K_{42} along each of the three best crystals of the third group; these crystals were grown in different experiments at 85 atm. The difference in the position and magnitude of the maximum thermal conductivity can be accounted for completely by small differences of crystal quality; the magnitude and temperature dependence of thermal conductivity in these crystals are otherwise in good agreement. On the other hand, as can be seen in Figs. 4a and 5a, there can be considerable differences between the thermal conductivities of different crystals grown under identical pressures and under approximately identical temperature conditions. These differences have the following causes:

- 1) Different degrees of single-crystal perfection (Fig. 6, for example).
- 2) Polycrystallinity.
- 3) Different concentrations of macroscopic impurities in the different experiments.
- 4) Different He^3 concentrations, which could affect the results of the second run, where all samples belong to groups II or III with regard to thermal conductivity.
- 5) The influence of He^4 lattice anisotropy on thermal conductivity. This possibility cannot be excluded because the orientation of crystals with respect to the vial axis is not identical, as a general rule, in different experiments. (Especially interesting are the crystals in which the high-temperature branches differ over the entire temperature range, while the low-temperature branches of the thermal conductivity practically

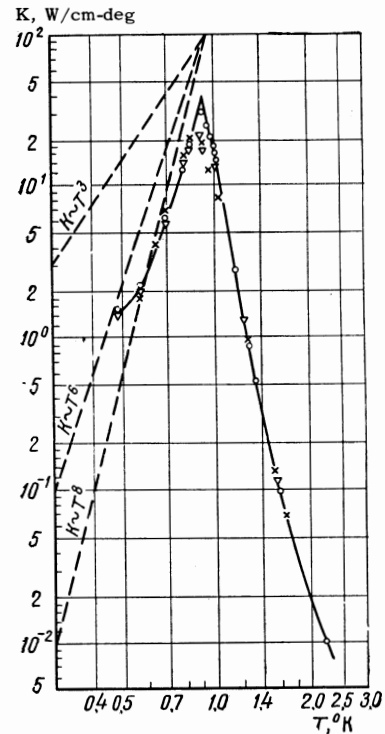


FIG. 6. A comparison of measurements for the best three crystals grown at 85 atm. Different power laws are here represented by the dashed lines.

coincide; examples are the crystals of groups I and II in Fig. 4a and groups I and III in Fig. 5a.)

Fairbank et al.^[2] observed a 20-fold increase of thermal conductivity following annealing (the dashed curves in Fig. 4a). However, we were unable to obtain essential improvement of crystal properties by the annealing process. For example, the crystal represented in Fig. 5b was maintained at 4.2°K, only 0.5° below its melting point, during a period of 10 hours. Yet the only result of this anneal was a small (15%) increase of K^{\max} in both parts of the crystal; all other results remained completely unchanged.

In a preliminary communication^[5] we reported data concerning the temperature jump at the copper-solid He^4 interface. The complex shape of this interface in our experiments prevented accurate measurements. However, assuming that the temperature jump here considerably exceeded the temperature gradient along the surface, we can estimate the parameters determining the required quantity. The temperature jump at the interface between the two media can be represented by

$$\Delta T = RQ,$$

where R is the Kapitza resistance. The magnitude and temperature dependence of R can vary somewhat even for identical crystals. Since

special experiments are anticipated to study the Kapitza jump at the helium-metal interface, we present here only the value obtained for one crystal grown at 185 atm:

$$R \approx 25 \cdot T^{-2.6} \text{ deg-cm}^2/\text{W}.$$

6. DISCUSSION OF EXPERIMENTAL RESULTS

Figure 7 shows the average thermal conductivity K_{42} of a crystal, measured on the best samples grown at 60, 85, 153,²⁾ and 185 atm (samples 1, 2, 3, and 4, respectively). Unfortunately, during the

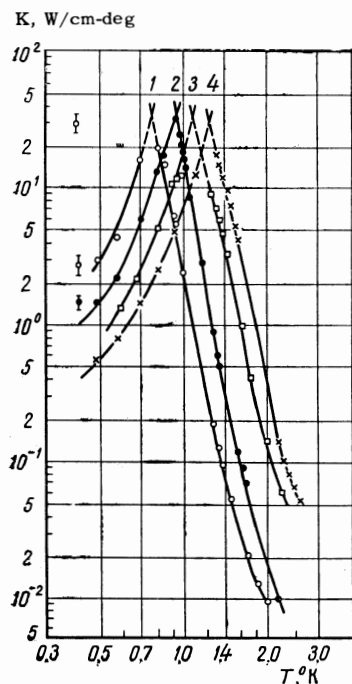


FIG. 7. Graphs for the best crystals grown at: 1 – 60 atm, 2 – 85 atm, 3 – 153 atm, and 4 – 185 atm.

experimental work it was difficult to determine the location of the thermal conductivity maximum; therefore, by analogy with the results at 85 atm, the maxima are here determined by extrapolating the high- and low-temperature branches—a procedure that is completely justified only for ideal crystals. All the crystals were grown as α He⁴ and therefore possess a hexagonal close-packed structure. The properties of these crystals are given in the accompanying table, where Θ is the Debye temperature and $V_{||}$ is the velocity of longitudinal vibrations.

²⁾Curve 3 is shown for the sake of completeness, since at 153 atm the crystals were investigated only in the first run. The graph shows that the presented result pertains to a crystal having a high concentration of defects.

The thermal conductivity of a dielectric crystal can be represented, as a general rule, by^[14]

$$K = \frac{1}{3} C V l_{\text{eff}} \quad (2)$$

where $C \sim (T/\Theta)^3$ is the heat capacity per unit volume, V is the mean velocity of sound, and l_{eff} is the effective mean free phonon path. Figure 8 shows the dependence of l_{eff} on the reduced temperature (T/Θ) calculated from (2). This calculation yields only the order of magnitude, especially since the Debye temperature varies as the temperature is reduced,^[12] and instead of the mean velocity we utilized the velocity of longitudinal vibrations in solid helium.^[13]

No.	P, atm	$\rho, \text{g/cm}^3$ [11]	$\Theta, \text{°K}$ [12]	$V_{ }, 10^4 \text{ cm/sec}$ [13]
1	60	0.209	31	6.2
2	85	0.218	34	6.9
3	153	0.237	41	8.2
4	185	0.244	43.5	8.8

Figures 6–8 show that the temperature dependence of thermal conductivity in the best samples does not behave as the simple theory predicts. First, the reduction of thermal conductivity at

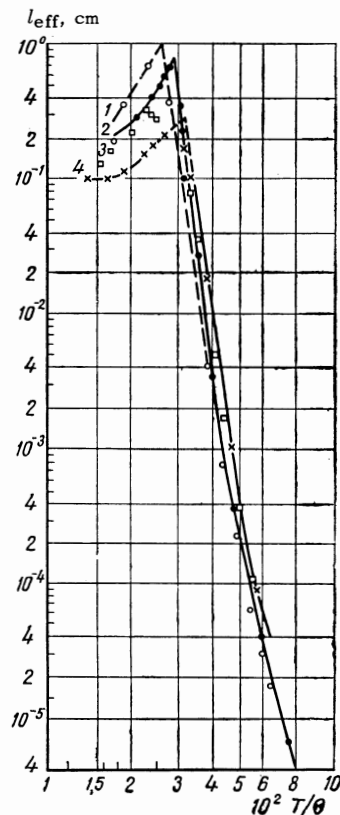


FIG. 8. Effective mean free phonon path vs. the reduced temperature T/Θ for all the crystals represented in Fig. 7.

lower temperatures after passing through the maximum differs from the $K \sim T^3$ law, and is described better by $K \sim T^n$, with n varying from $\sim 6-8$ near the maximum to ~ 3 at the lowest temperatures. Secondly, it follows from Fig. 8 that the maximum effective mean free phonon path can be several times longer than the diameter of the sample.

The behavior of the thermal conductivity of He^4 crystals that we observed was found to be in unexpectedly good agreement with the theory of Gurzhi,^[15] who calculated anew the effect of normal (without momentum loss) collisions on transport processes in bulk single crystals. The normal processes do not alter qualitatively the results associated with spatial collisions involving momentum losses (U processes and impurity scattering). However, they can greatly change the order of magnitude of thermal conductivity and its dependence on sample size and on temperature in the temperature region where thermal resistance results from Coulomb scattering at the sample boundaries or macroscopic distortions. In a very pure bulk sample at low temperatures we have the inequality

$$l_{pp}^N \ll d \ll l_{pp}^V, \quad (3)$$

where l_{pp}^V is an effective length characterizing spatial collisions with momentum loss, l_{pp}^N is the effective mean free phonon path in normal collisions, and d is a characteristic sample dimension. Moving like a Brownian particle, a phonon traverses a path l_{eff} of the order d^2/l_{pp}^N between two collisions with the boundaries, and from (2) we have in this region

$$K \sim CVd^2/l_{pp}^N. \quad (4)$$

Figure 9 shows a typical temperature dependence of dielectric thermal conductivity in the Gurzhi model; the usual temperature dependence is represented by dashed curve. At the lowest temperatures with $l_{pp}^N \gg d$ we obviously have $l_{\text{eff}} \sim d$ and

$$K \sim CVd \sim da^{-3}V(T/\Theta)^3 \quad (5)$$

where a is the lattice constant and $\Theta \sim hV/a$. From the temperature T_1 at which $l_{pp}^N \sim d$ to T_2 at which $d^2/l_{pp}^N \sim l^V$ a diffusion mechanism plays the principal role and

$$K \sim CV(d^2/l_{pp}^N) \sim (\Theta/MV)(d^2/a^4)(T/\Theta)^8. \quad (6)$$

Beyond this range the usual decline of thermal conductivity is observed; this decrease is exponential when U processes predominate, or obeys a $1/T$ law when scattering by point defects is

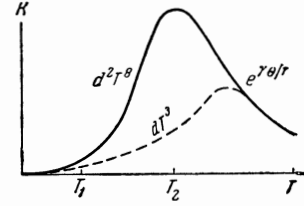


FIG. 9. Temperature dependence of thermal conductivity in an ideal dielectric according to the Gurzhi model. The dashed curve represents the temperature dependence that is usually observed.

most important. The predicted behavior of thermal conductivity (Fig. 9) is seen to be in good agreement with our observations (Figs. 6 and 7).

We have, in order of magnitude,

$$l_{pp}^N \sim a(MV^2/\Theta)(\Theta/T)^5, \quad (7)$$

where M is the atomic mass, and

$$l_{pp}^V \sim a(MV^2/\Theta)(T/\Theta)^{1/2} \exp(\gamma\Theta/T). \quad (8)$$

It has been shown by the author that the numerical value of γ depends on the behavior of the phonon spectrum within the entire Brillouin cell, for otherwise the given result, including the factor $(T/\Theta)^{5/2}$, is independent of the kind of dispersion law. For all samples shown in Fig. 7 calculations employing (8) lead to $1/\gamma = 1.76 \pm 0.06$. It follows from (3)–(8) that the diffusion mechanism manifests itself most clearly in sufficiently massive samples, and at the lowest Debye temperatures in crystals having equal diameters.

Figure 8 shows that, in agreement with the theory, as Θ decreases the high- and low-temperature branches are shifted to lower values of the reduced temperature T/Θ ; at the same time there is a broadening of the temperature range in which the diffusion mechanism can be operative. Unfortunately, at the lowest temperatures the measurements are insufficiently accurate to indicate the further behavior of the low-temperature branches as the temperature is lowered. It follows from general considerations that at sufficiently low temperatures the values of l_{eff} should agree for all crystals.

In insufficiently perfect samples scattering by lattice defects can also be important. Macroscopic defects (crystal boundaries and foreign particles) limit the phonon mean free path at the lowest temperatures:

$$l_{\text{eff}} \sim d_i, \quad (9)$$

where d_i is the mean separation of macroscopic defects, whose influence can thus be evaluated easily from the shifted position of the low-temperature branch of the thermal conductivity curve

(for example, from the enhanced thermal conductivity of annealed samples in Fairbank's experiments). A greater concentration of macroscopic defects can also account for the different positions of the low-temperature branches in some of our experiments (for example, in a crystal of group III in Fig. 4a or of group II in Fig. 5a). Point defects affect principally the behavior of the high-temperature branch. The corresponding mean free path is

$$l_{pi} \sim (a/c)(\Theta/T)^4 \quad (10)$$

where c is the concentration of point defects; then

$$(l^V)^{-1} = (l_{pp}^U)^{-1} + (l_{pi})^{-1}, \quad (11)$$

where l^V is an effective length characterizing spatial collisions with momentum loss, l_p^U is the mean free path in inelastic phonon-phonon scattering, l_{pi} is the mean free path in inelastic phonon scattering by point defects. At higher concentrations of point defects there is an expansion of the temperature range near the thermal conductivity maximum where the exponential variation of thermal conductivity (associated with U processes) is replaced by a much weaker power law. The nonidentical behavior of the thermal conductivity of the crystals shown in Fig. 6 is fully accounted for by different concentrations of microscopic defects in these crystals. However, this explanation does not apply to crystals in which the low-temperature branches coincide while the high-temperature branches differ appreciably in the entire temperature interval, because with the exception of a narrow temperature interval near the maximum the high-temperature branches of all the investigated samples obey exponential rather than power laws. The most likely explanation of the differences in the behavior of the high-temperature branches of these crystals lies in the unequal numerical values of the parameter γ in Eq. (8) for different crystallographic directions, especially since in the different experiments the crystals did not have the same orientation with respect to the axis of the vial.

7. CONCLUSION

It was our aim to prepare and investigate perfect single crystals of solid He⁴. The utilized technique of growing crystals under constant pressure with continuous visual and temperature control appears to produce crystals of very high quality. The calculated mean free path indicates

that at least one-third of the samples grown in the last series of experiments are single crystals having a low concentration of lattice defects. The temperature dependence and the maximum thermal conductivity of these crystals differ greatly from the usual observations, and agree closely with the results obtained in Gurzhi's theoretical investigation of transport processes in ideal crystals.

As indicated in the preceding section, the diffusion mechanism of phonon-phonon scattering is observed most clearly in very much elongated crystals; for higher Debye temperatures the characteristic diameters of the samples increase. Solid helium is an especially convenient object of investigation, because its Debye temperature in the investigated pressure interval is several times smaller than Θ for ordinary dielectrics. The region of diffusive phonon scattering is of interest in connection with the possibility of exciting second sound in crystals. Gurzhi has shown that N -processes lead only to the internal equilibrium of phonons in each volume element (much larger than l_{pp}^N) that can move as a whole through the crystal. This means that in the temperature region where $l_{pp}^N \ll d \ll l^V$ thermal waves can be excited in a crystal with wavelengths satisfying the condition $l_{pp}^N \ll \lambda \lesssim d$. Calculations show that this condition corresponds to a frequency $\sim 10^5$ cps/sec, so that it would be very difficult to observe second sound directly in solid helium.

The author is indebted to P. L. Kapitza for the opportunity of doing the present work at the Institute for Physics Problems and for his interest, to A. I. Shal'nikov for his continued interest and valuable advice after suggesting the problem, to D. I. Vasil'ev for experimental assistance, and to R. N. Gurzhi for valuable discussions.

¹ Webb, Wilkinson, and Wilks, Proc. Roy. Soc. (London) **A214**, 546 (1952); K. R. Wilkinson and J. Wilks, Proc. Phys. Soc. (London) **64A**, 89 (1951); F. J. Webb and J. Wilks, Phil. Mag. **44**, 663 (1953).

² J. E. Walker and H. A. Fairbank, Phys. Rev. Letters **5**, 139 (1960); M. J. Crooks and H. A. Fairbank, Proc. of the Eighth International Conference on Low Temperature Physics, London, 1962.

³ A. I. Shal'nikov, JETP **41**, 1056 (1961), Soviet Phys. JETP **14**, 753 (1962).

⁴ A. I. Shal'nikov, JETP **41**, 1059 (1961), Soviet Phys. JETP **14**, 755 (1962).

⁵ L. P. Mezhov-Deglin, JETP **46**, 1926 (1964), Soviet Phys. JETP **19**, 1297 (1964).

⁶ V. K. Tkachenko and A. I. Filimonov, PTÉ No. 5, 203 (1961).

⁷ D. I. Vasil'ev, PTÉ (in press).

⁸ Peshkov, Zinov'eva, and Filimonov, JETP 36, 1034 (1959), Soviet Phys. JETP 9, 734 (1959).

⁹ J. R. Clement and E. H. Quinell, Rev. Sci. Instr. 23, 213 (1952).

¹⁰ A. N. Vetchinkin, PTÉ No. 1, 192 (1961).

¹¹ J. S. Dugdale, and F. E. Simon, Proc. Roy. Soc. A218, 291 (1953).

¹² E. C. Heltemes and C. A. Swenson, Phys. Rev. 128, 1512 (1962).

¹³ J. H. Vignos and H. A. Fairbanks, op. cit. ref.^[2], p. 31.

¹⁴ R. E. Peierls, Quantum Theory of Solids, Clarendon Press, Oxford, 1955 (Russ. transl., IIL, Moscow, 1956).

¹⁵ R. N. Gurzhi, JETP 46, 719 (1964), Soviet Phys. JETP 19, 490 (1964).

Translated by I. Emin